ONLINE ESTIMATION OF WHEEL SINKAGE AND SLIPPAGE USING A TOF CAMERA ON LOOSE SOIL

Shoya Higa[a], Kenji Nagaoka[a], and Kazuya Yoshida[a]

[a] *Tohoku University, Aoba 6-6-01, Aramaki, Aoba-ku, Sendai, 980-8579, Japan*
shoya@astro.mech.tohoku.ac.jp, nagaoka@astro.mech.tohoku.ac.jp, yoshida@astro.mech.tohoku.ac.jp

Abstract
A prominent concern of a wheeled mobile robot that travels on loose and rough terrain is to get stuck in soil, which is brought with a sharp increase in wheel sinkage and slippage. For this issue, various analyses of wheel-soil interaction mechanics have been conducted until now. Several studies on online estimation of the wheel sinkage and slippage using image processing have been conducted. However, these image-based online estimation methods are greatly affected by conditions of target environment such as lighting or reflectance. In contrast, a ranging sensor of three-dimensional point cloud data performs better for the estimation even in an uncertain environment. In this study, we proposed the online sinkage/slippage estimation method using a time-of-flight (ToF) camera that can measure the distance from a target object. By attaching the ToF camera on the side of the wheel, we experimentally demonstrated the sinkage/slippage estimation of the traveling wheel on loose soil. The experimental result provided that the wheel sinkage can be estimated precisely using the point cloud data, and the slippage can also be done less than 3.9% as an absolute error.

Keywords: Online estimation, Sinkage, Slippage, Lunar/planetary exploration rover

1. Introduction

Lunar or Martian surfaces are basically covered with fine regolith, gravel, and rocks. In the past lunar/planetary exploration missions using unmanned mobile rovers, rigid metallic wheels have been mainly adopted as their locomotion gears. Wheel mechanism excels in mobility performance and has mechanical simplicity.

However, wheel sinkage and slippage are induced particularly when traversing over loose soil. These phenomena adversely affect robotic operations. For such unmanned missions, a worst-case scenario is that the wheel buries into the loose soil, and the rover gets stuck. Wheel sinkage and slippage induce this scenario. To reduce the wheel slippage, several studies on mechanistic improvements or motion control have ever been addressed. In particular, the design of a larger wheel and using plate-like lugs or grousers on the wheel surface is effective means for the mechanistic improvements (Sutoh et al., 2013, 2012).

Getting stuck is induced with a sharp increase in the wheel sinkage and slippage as shown in Fig. 1. To avoid getting stuck, each wheel of the rover needs to estimate its traveling conditions in rough terrain independently. As a goal of this study, we, therefore, aim at the development of a new intelligent wheel system that can achieve an online estimation of the wheel sinkage and slippage. We have focused attention on wheel-soil interaction mechanics and have ever reviewed on a key mechanical relationship between contact forces acting on the wheel from the soil, the wheel sinkage, and slippage.

In the field of terramechanics, the contact forces such as normal force or drawbar pull were modeled based on the normal and shear stress distribution generated at contact patch with the soil. However, these conventional models target heavyweight vehicles such as large-scale construction machines, agricultural vehicles, or military vehicles. Thus, small and lightweight vehicles like lunar/planetary exploration rovers are out of their applicable scope. Therefore, we have

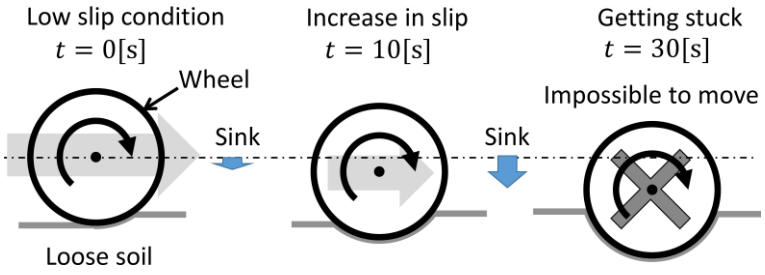

Fig. 1 Getting stuck mechanism.

ever measured the stress distributions generated beneath a wheel in detail to re-model the stress distributions of small rovers. We developed a novel stress measurement system that can measure three-axial stress distributions at the contact patch. In the measurement system, a six-axis force and torque sensor is attached inside the wheel, which can measure the stresses at a specific sensing area on the wheel surface by a specialized contact-part. By integrating several measurement results, we obtained the three-axial stress distributions with the wheel rotation angles. The measurement results showed the more precise stress distributions, and we also discussed the validity of them by analyzing the equilibrium of wheel weight and the resulting normal force (Higa et al., 2015).

From the achievement and knowledge by our previous works, we found that the stress distribution is influenced by the wheel sinkage, slippage, and terrain conditions, and it becomes different characteristics. That is if we can estimate the force acting on the wheel, the terrain conditions and the wheel sinkage/slippage is expected to be estimated as well. However, this measurement method of the three-dimensional stress distribution cannot always measure the entire stress distribution throughout wheel rotation. Hence, it was difficult to attempt to apply this method to the robotic missions that the rover travels with the continuous online estimation of the sinkage and slippage based on on-board measurement. Therefore, to realize the online estimation of the wheel conditions (e.g., the forces and torques, the wheel sinkage, and the wheel slippage) in the actual environment, a novel stress distribution model based on three-dimensional stress measurement results is required for that online estimation.

As related works, Iagnemma et al. (2004) addressed online estimation of terrain parameters by reflecting the force acting on the wheel into the conventional model. This approach was accomplished by sensing the reaction forces on a mobile robot from the terrain. Nagatani et al. (2009) accurately estimated the drawbar pull by directly measuring the normal stress distribution beneath the wheel using force sensor arrays on its surface. From these related works, the direct measurement of the forces and torques acting on the wheel is more effective for performing better-wheeled mobility on the unknown rough terrain. We thus propose the intelligent wheel that can online estimate the force/torque acting on the wheel and the wheel sinkage and slippage. We conclusively aim to realize that avoid getting stuck by implementing the velocity distribution control using intelligent wheels. As a first step for the smart wheel, we address the development of the measurement system that allows for online estimate the wheel sinkage and slippage.

In this paper, we first describe a concept of intelligent wheel system. Then, we present a single wheel testbed developed for comprehensive wheel traveling experiments on loose soil. Finally, the estimation results of the wheel sinkage/slippage using a time-of-flight (ToF) camera, which can measure the distance from a target object, are presented based on traveling experiments. The ToF camera-based estimation method shows better performance of the estimation on loose soil, and this can be used for various field robot applications.

2. Concept of Intelligent Wheel System

Figure 2 shows a conceptual diagram of an intelligent wheel system. The intelligent wheel is mainly composed of a wheel (with a rotary motor for its driving), a ToF camera, and a six-axis force and torque (F/T) sensor. For the online estimation of the wheel sinkage and slippage, we used a ToF camera. The ToF camera outputs point cloud data of distance between a sensing IC of the ToF camera and a target object. Calculation cost of the distance is low because of an onboard processor specialized for the distance calculation. The ToF camera can also capture an 8bit/16bit monochrome image. Hence, the wheel slippage estimation is performed based on optical flow technique. The intelligent wheel can measure the forces and torques by the six-axis F/T sensor attached on a wheel's rotation axis and on between the wheel and its driving motor. Moreover, combining the rover attitude data measured from an IMU (Internal Measurement Unit) inside the rover, more accurate estimation of the wheel and terrain conditions can be achieved.

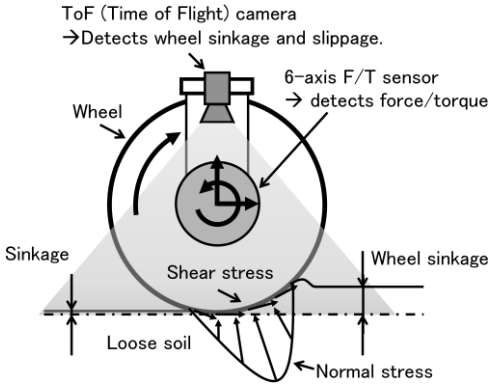

Fig. 2 Conceptual diagram of an intelligent wheel.

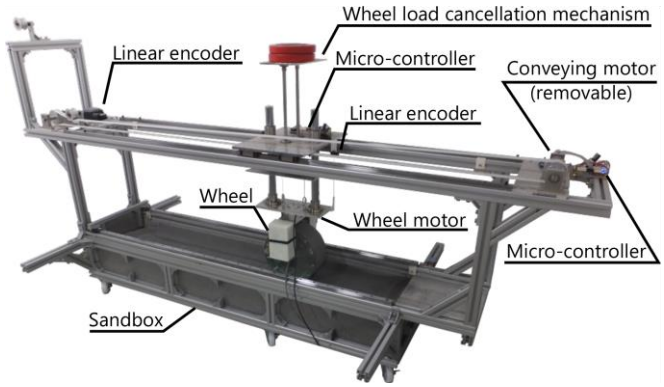

Fig. 3 Overview of the single wheel testbed.

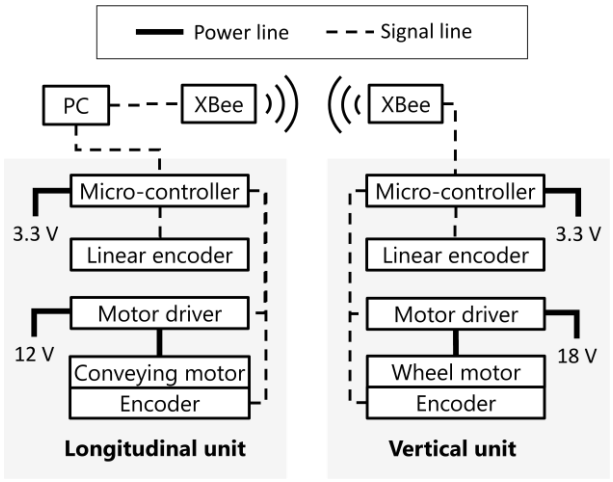

Fig. 4 System diagram of the single wheel testbed.

The intelligent wheel system developed in this study estimates the forces/torques acting on the wheel by using the F/T sensor data. Moreover, it allows estimating the wheel sinkage and slippage online throughout traveling by which the ToF camera is attached on the outside of the wheel.

In this paper, we focus on the online wheel sinkage/slippage estimation for the intelligent wheel.

3. Single Wheel Testbed

For comprehensive traveling experiments of a wheel on loose soil, we developed a single wheel testbed. Figure 3 shows an overview of the single wheel testbed. The size of the testbed, which includes the sandbox, is 2.50 m in length, 1.05 m in width, and 1.25 m in height. The length, width, and height of the sandbox are also 1.6 m, 0.3 m, and 0.2 m, respectively. In our laboratory, we have two sandboxes whose size are same and are filled with Toyoura standard sand and lunar regolith simulant in each. Hence, we can carry out traveling experiment using different soils by just replacing the sandbox.

The testbed is composed of a longitudinal unit restricted to a horizontal traveling direction via a linear guide, and a vertical unit restricted to a vertical direction via a linear shaft and freely move along the vertical direction. We designed the testbed based on static structure analysis so that the wheel weight of 100 N can be applied. In the testbed, the wheel diameter of 250 mm can travel on test soil up to 85 mm in sinkage. Furthermore, the wheel load can also be adjusted by the load canceller mechanism.

On the other hand, the longitudinal unit is connected to a conveying motor for horizontal movement via timing pulleys and a belt. The conveying motor and timing pulleys are also connected via a shaft coupling, where this connection is removable. Therefore, we can simulate two traveling conditions: a forced slip condition by the conveying

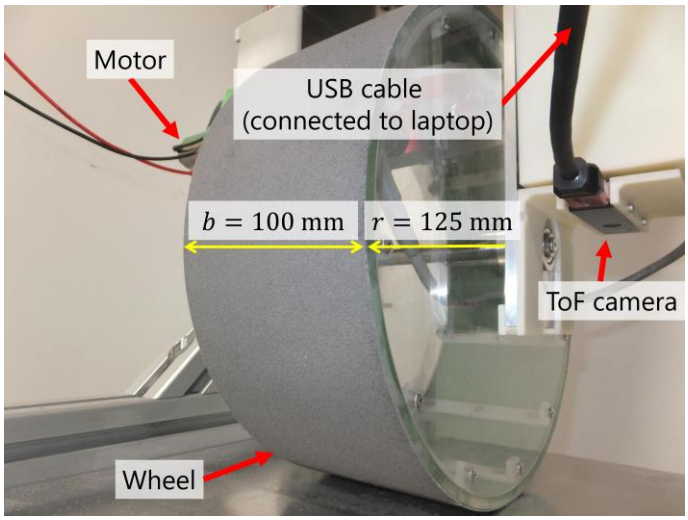

Fig. 5 The wheel configuration for online sinkage/slippage estimation.

motor, and a free slip condition by constant traction load. In the latter case, we additionally connect a traction rope to the timing belt and hook up several traction load as to traveling conditions.

Figure 4 shows the system diagram of the single wheel testbed. The wheel rotates by a rotary DC motor with a harmonic drive gear, and its final gear ratio is 750:1. The wheel motor is connected to a micro-controller via a motor driver, and can perform constant wheel rotational velocity by a feedback controller. The vertical unit is conveyed using the conveying motor or the traction load in the horizontal direction. The conveying motor is also controlled to keep constant horizontal traveling velocity using a micro-controller. Wireless serial communication using the XBee modules is used for sending commands and receiving the data between PC and the microcontroller of the vertical unit. The linear encoder of the vertical and longitudinal unit counts the wheel sinkage and wheel traveling distance, respectively. The measurement data obtained by the linear encoders is used for ground truth of the wheel trajectory and not utilized for the online estimation.

4. Online Estimation of Wheel Sinkage

As related works, a visual odometry system using a telecentric camera on loose soil (Nagatani et al., 2010) was studied. The wheel sinkage/slippage estimation based on image processing by captured images on the side surface of the traveling wheel (Milella et al., 2006; Reina et al., 2006) were also studied. Image-based estimation of soil's physical properties has very sensitive to depending on environmental conditions such as intensity of lighting conditions. In contrast, more robust estimation of the wheel sinkage to such environmental uncertainties can be achieved by a ToF camera because it provides three-dimensional point cloud ranging data. In this section, we present online wheel sinkage estimation using a ToF camera toward the development of the intelligent wheel.

4.1 Wheel Configuration

Figure 5 shows the test wheel utilized in this study. The wheel weighs 50 N and is connected to a DC motor via the timing belt. The wheel is also controlled so that its rotational velocity keeps constant by a micro-controller. The wheel diameter and width are 250 and 100 mm, respectively. In this study, we attached a ToF camera "CamBoard pico flex" produced by PMD Technologies AG in the side position of the wheel as shown in Fig. 5, and carried out traveling experiments for the online wheel sinkage estimation. The ToF camera can sense 100 mm in depth as its minimum ranging distance. The point cloud ranging data can be obtained by utilizing an infrared light flashed from the camera. It was also connected via USB communication to an operation PC. Sinkage calculation was conducted on the PC based on the point could data received from the ToF camera.

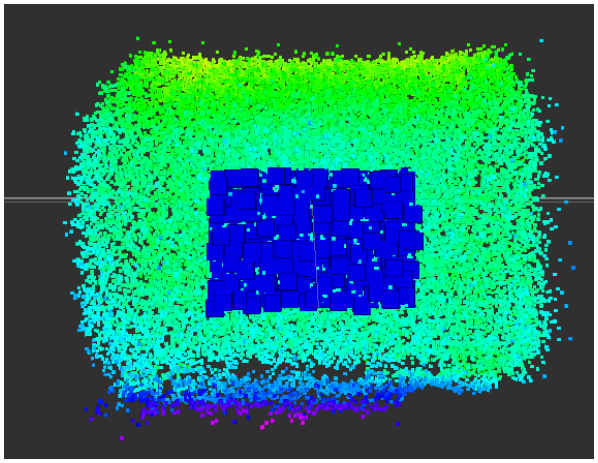

Fig. 6 Point cloud data obtained by the ToF camera.

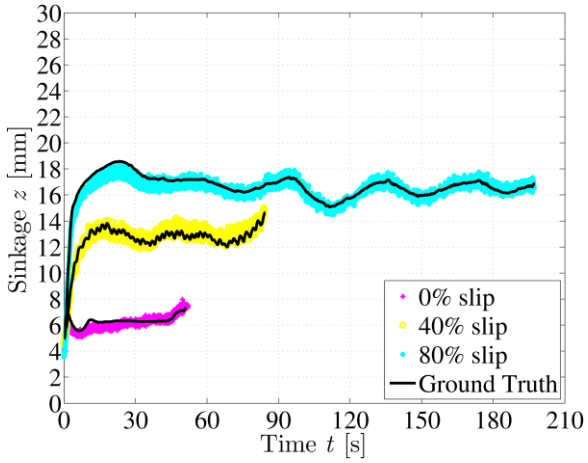

Fig. 7 Estimation results of the wheel sinkage.

4.2 Experimental Conditions

In this study, we estimated the wheel sinkage using the three-dimensional point cloud data by the following procedures:

1. Extract point cloud data in the region of interest using a Pass Through filter.
2. Down-sample the point cloud data using a Voxel Grid filter.
3. Calculate the arithmetic mean of the point cloud data.
4. Calculate the wheel sinkage from the geometric relationship between the origin coordinate of ToF camera and wheel.

We compared the results of the wheel sinkage calculated by the estimation method and measured by the linear encoder of the vertical unit. Here, the target circumferential velocity at the wheel rim was controlled to be 20 mm/s. The comparative analysis of the wheel sinkage was performed under three different slip ratio: 0%, 40%, and 80%. We at this moment introduce the slip ratio s as an evaluation index as follows:

$$s = \left(1 - \frac{v_x}{r\omega}\right) \times 100 \tag{1}$$

where v_x is the traveling velocity of the wheel, r is the wheel radius, ω is the wheel angular velocity.

Slip ratio is expressed by the ratio between the actual traveling and circumferential velocity of the wheel. In a general case of a driving wheel, the slip ratio becomes a positive value from 0 to 100 in percentage. In case $s = 0$ [%], it corresponds to which the wheel travels without any slippage, and in case $s = 100$ [%], it does to which the wheel completely slips and gets stuck.

Furthermore, we used a fine lunar regolith simulant FJS-1 (Kanamori et al., 1998) as the test soil. The soil in the sandbox was mixed loosely and then made flat before each traveling experiment. Compared to Toyoura standard sand, an optical reflection of FJS-1 becomes smaller.

4.3 Results and Discussions

Figure 6 shows the resulting point cloud data of the ranging distance obtained by the ToF camera. The blue region was extracted by the procedure 1 and 2. Figure 7 also depicts the time histories of the estimation results of the wheel sinkage over the wheel traveling time and the ground truth measured by the linear encoders of the longitudinal unit. The results confirm the estimated sinkage was better matched with the ground truth regardless of the slip ratio. The estimation error was less than 2 mm. In the sinkage estimation method using the ToF camera, we calculated the average value of the point cloud data in the extracted region. Also, from a viewpoint of an intelligent data analysis, a probabilistic filtering approach will be fostered to accomplish more accurate estimation.

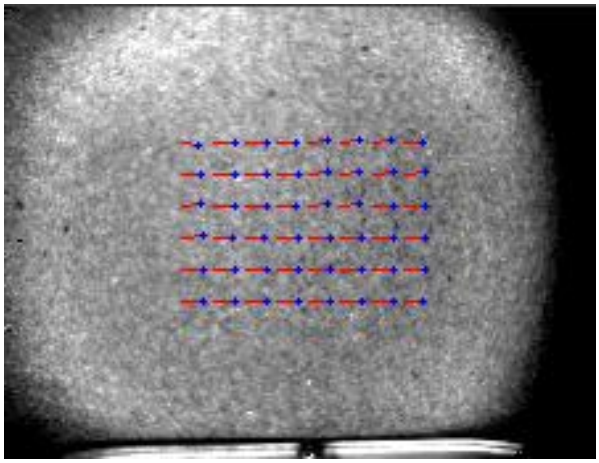

Fig. 8 Snapshot of optical flow calculation ($s = 0$ [%]).

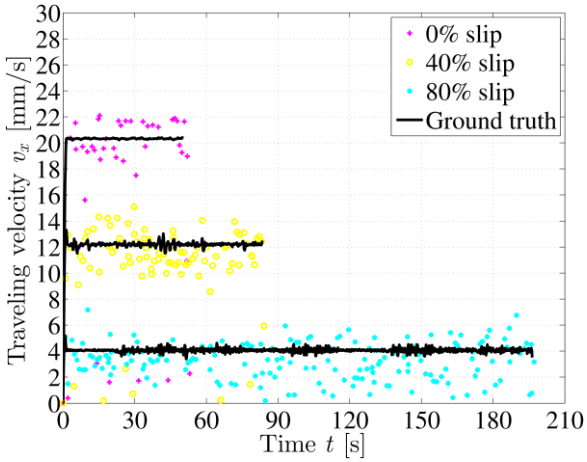

Fig. 9 Estimation result of traveling velocity.

5. Online Estimation of Wheel Slippage

The online estimation of the wheel slippage is one of the key technical challenges for a wheeled mobile robot on loose soil. The ToF camera provides an 8-bit monochrome image in addition to the point cloud ranging data. The image can also be obtained by the use of the infrared light. Thus, the image obtained by the ToF camera is not influenced by environmental lighting conditions but cannot discriminate color information of target objects. The image size is 224×171 pixel. Although this is a low resolution as a camera, it is enough to track soil particles at close-range from the wheel. By these, we estimated the wheel slippage by applying an optical flow technique to the images.

5.1 Estimation Method of Wheel Slippage

According to the definition of wheel slip ratio in Eq. (1), the circumferential velocity of the wheel can be calculated by the wheel radius and encoder of the wheel motor. For an estimate of the wheel traveling velocity, the actual traveling velocity of the wheel under several slip ratios is required. Although the ToF camera provides the point cloud data, it is difficult to estimate the wheel traveling velocity using the data. To estimate the wheel traveling velocity using the point cloud data, apparent features in target environment are essential. We, therefore, proposed an estimation method of the wheel traveling velocity applying an optical flow technique to the monochrome images.

In general, we can use two typical optical flow techniques. One is called sparse optical flow techniques (e.g., the Lucas-Kanade algorithm (Bouguet, 1999)), and the other is dense optical flow techniques (e.g., the Farneback algorithm (Farnebäck, 2003)). The former techniques preliminarily detect features of an image and then track the movement of each feature. Their advantage is low calculation cost. However, the feature extraction becomes more challenging for a ToF camera because it flashes an infrared light when obtaining images. We, therefore, used the latter method for the slippage estimation. Although higher calculation cost of the latter method because we must calculate all pixels as averaging several pixels, such a concern of the cost mainly occurs when we use high definition images. To reduce the calculation cost, we estimated the wheel traveling velocity as follows:

1. Mask the image by a region of interest.
2. Calculate optical flows using the Farneback algorithm.
3. Display arrows on the features by averaging 12×12 pixels.
4. Calculate the traveling velocity by inputting the distance to the soil surface.
5. Calculate the wheel slippage based on Eq. (1).

The experiments were carried under the same conditions as the experiments for the wheel sinkage estimation. The ground truth data of the wheel slippage was measured by the encoders of both the wheel motor and the conveying motor. These motors were controlled to be constant rotational velocity during the experiments. To reduce an effect of image distortion, we only used a center region of the image. The averaging sinkage value at near area was also applied.

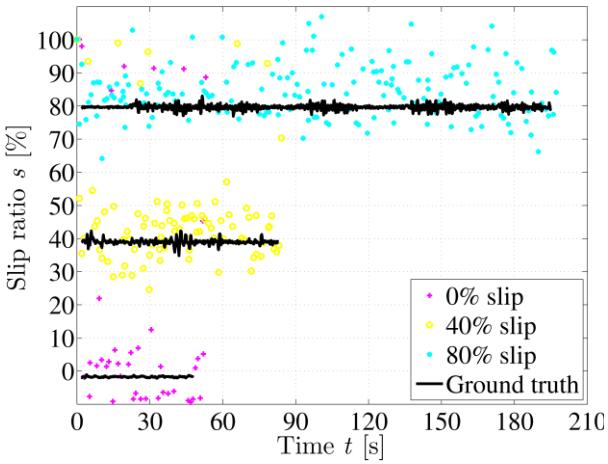

Fig. 10 Estimation result of each slip ratio.

5.2 Calculation of Traveling velocity

The optical flow algorithm provides distance between two images. To calculate the traveling velocity v_x, we need to know actual length of each pixel. Actual length of each pixel can be obtain by relationship between the view angle and the resolution of the ToF camera. In this study, we simply calculated the traveling velocity as follows:

$$v_x = z_d \tan\frac{\theta_H}{2} \cdot \frac{\Delta x}{\Delta t}. \tag{2}$$

where z_d is the distance between the origin of the ToF camera and the soil surface, θ_H is the viewing angle in the horizontal axis of the ToF camera, Δx is average distance provided by an optical flow, and Δt is interval time between each image. Eq. (2) means conversion from pixel velocity of the images to the traveling velocity.

5.3 Results and Discussion

Figure 8 shows a snapshot of the optical flow technique under $s = 0$ [%]. The result confirm that the soil particles were better tracked based on the optical flow. Each line shows distance between two images and each plot shows current position of tracked pixel block. Therefore, this result means that the soil moves to left direction of the image.

Figure 9 depicts the estimates of the traveling velocity of the wheel in steady state over the traveling time. Each black line shows the time histories of the ground truth data by the linear encoder. Each plot does the ones of the estimated traveling velocity. Most of the estimates quantitatively vary but can reflect their qualitative tendency. Table 1 lists median values of each estimated traveling velocity and their absolute errors. The results show that the absolute errors between the target velocity and estimated velocity are less than 0.7 mm/s. Thus, we conclude that traveling velocity can be estimated with 1 mm/s order resolution.

Figure 10 shows the slip ratio of the wheel using estimated traveling velocity shown in Figure 9 and Table 1. To validate the estimated wheel slippage, we calculated the median value of each estimated slip ratio under the steady state condition. Table 2 shows median values of each estimated wheel slippage and their absolute errors. Although estimated traveling velocity under large slip ratio was less accurate, their absolute errors of each slip ratio are less than 3.9%. In particular, the absolute error indicated 1.4% at smaller slip ratio. We, therefore, conclude that the wheel slippage can be estimated precisely, and the proposed method is validated for the online estimation of wheel slippage.

Table 1 Estimation results of the traveling velocity.

Slip ratio [%]	Target velocity [mm/s]	Estimated velocity [mm/s]	Absolute error [mm/s]
0	20	19.5	0.5
40	12	11.3	0.7
80	4	3.3	0.7

6. Conclusion

In this study, we online estimated the wheel sinkage and slippage only using a ToF camera as a first step for the development of the intelligent wheel. From the estimation results, we showed that the sinkage can be estimated precisely using the ToF camera that has millimeter order space resolution. Traveling velocities of the wheel were estimated with 1 mm/s order resolution. Moreover, the wheel slippage was estimated less than an absolute error of 3.9%.

For future works, the attachment position of the ToF camera will be examined to enhance estimation accuracy. In addition to this, a six-axis F/T sensor is introduced to the wheel, and we attempt to estimate terrain conditions or soil characteristics by measurement of force and torque data acting on the wheel's rotational axis.

Nomenclature

s	Slip ratio	[%]
r	Wheel radius	[mm]
v_x	Wheel traveling velocity	[mm/s]
ω	Wheel angular velocity	[rad/s]
z_d	Distance to the soil surface	[mm]
θ_H	Horizontal view angle	[°]
Δx	Average distance	[mm]
Δt	Interval time	[s]

Acknowledgements

This research was partially supported by Grant-in-Aid for JSPS Fellows (Grant Number 16J02425).

References

Bouguet, J.-Y., 1999. Pyramidal implementation of the affine lucas kanade feature tracker-description of the algorithm, Technical report, OpenCV Document.

Farnebäck, G., 2003. Two-Frame Motion Estimation Based on Polynomial Expansion, in: Image Analysis, Proceedings. pp. 363–370. doi:10.1007/3-540-45103-X_50

Higa, S., Sawada, K., Nagaoka, K., Nagatani, K., Yoshida, K., 2015. Three-dimensional stress distribution on a rigid wheel surface for a lightweight vehicle, in: Proceedings of the 13th European Conference of the ISTVS. Rome, Italy, pp. 383–391.

Iagnemma, K., Kang, S., Shibly, H., Dubowsky, S., 2004. Online Terrain Parameter Estimation for Wheeled Mobile Robots With Application to Planetary Rovers. IEEE Transactions on Robotics 20, 921–927. doi:10.1109/TRO.2004.829462

Kanamori, H., Udagawa, S., Yoshida, T., Matsumoto, S., Takagi, K., 1998. Properties of Lunar Soil Simulant Manufactured in Japan. Space 98 (6th), April 26-30 462–468. doi:10.1061/40339(206)53

Milella, A., Reina, G., Siegwart, R., 2006. Computer Vision Methods for Improved Mobile Robot State Estimation in Challenging Terrains. Journal of Multimedia 1, 49–61. doi:10.4304/jmm.1.7.49-61

Table 2 Estimation results of the wheel slippage.

Target slip ratio [%]	Estimated slip ratio [%]	Absolute error [%]
0	1.4	1.4
40	43.4	3.4
80	83.9	3.9

Nagatani, K., Ikeda, A., Ishigami, G., Yoshida, K., Nagai, I., 2010. Development of a Visual Odometry System for a Wheeled Robot on Loose Soil using a Telecentric Camera. Advanced Robotics 24, 1149–1167. doi:10.1163/016918610X501282

Nagatani, K., Ikeda, A., Sato, K., Yoshida, K., 2009. Accurate estimation of drawbar pull of wheeled mobile robots traversing sandy terrain using built-in force sensor array wheel, in: 2009 IEEE/RSJ International Conference on Intelligent Robots and Systems. IEEE, pp. 2373–2378. doi:10.1109/IROS.2009.5354566

Reina, G., Ojeda, L., Milella, A., Borenstein, J., 2006. Wheel slippage and sinkage detection for planetary rovers. IEEE/ASME Transactions on Mechatronics 11, 185–195. doi:10.1109/TMECH.2006.871095

Sutoh, M., Nagaoka, K., Nagatani, K., Yoshida, K., 2013. Design of wheels with grousers for planetary rovers traveling over loose soil. Journal of Terramechanics 50, 345–353. doi:10.1016/j.jterra.2013.05.002

Sutoh, M., Yusa, J., Ito, T., Nagatani, K., Yoshida, K., 2012. Traveling performance evaluation of planetary rovers on loose soil. Journal of Field Robotics 29, 648–662. doi:10.1002/rob.21405